Journal of Solid State Chemistry 183 (2010) 402–407

Contents lists available at ScienceDirect

Journal of Solid State Chemistry

journal homepage: www.elsevier.com/locate/jssc

High-pressure crystal growth and magnetic and electrical properties of the quasi-one dimensional osmium oxide Na_2OsO_4

Y.G. Shi [a,b], Y.F. Guo [a,b], S. Yu [b,c], M. Arai [d], A.A. Belik [a,b], A. Sato [e], K. Yamaura [b,c,f,*], E. Takayama-Muromachi [a,b,c,f], T. Varga [g,1], J.F. Mitchell [g]

[a] International Center for Materials Nanoarchitectonics (MANA), National Institute for Materials Science, Tsukuba, Ibaraki 305-0044, Japan
[b] JST, Transformative Research-Project on Iron Pnictides (TRIP), 5 Sanbancho, chiyoda-ku, Tokyo 102-0075, Japan
[c] Superconducting Materials Center, National Institute for Materials Science, 1-1 Namiki, Tsukuba, 305-0044 Ibaraki, Japan
[d] Computational Materials Science Center, National Institute for Materials Science, 1-1 Namiki, Tsukuba, Ibaraki 305-0044, Japan
[e] Materials Analysis Station, National Institute for Materials Science, 1-1 Namiki, Tsukuba, Ibaraki 305-0044, Japan
[f] Department of Chemistry, Graduate School of Science, Hokkaido University, Sapporo, Hokkaido 060-0810, Japan
[g] Materials Science Division, Argonne National Laboratory, 9700 South Cass Avenue, Argonne, IL 60439, USA

ARTICLE INFO

Article history:
Received 7 October 2009
Received in revised form
24 November 2009
Accepted 7 December 2009
Available online 16 December 2009

Keywords:
Ca_2IrO_4
High pressure synthesis
Osmium oxides

ABSTRACT

Na_2OsO_4 crystals were grown by a NaCl flux method under high pressure. It crystallizes in the Ca_2IrO_4-type structure without having additional elements or metal vacancies, which are usually accommodated. It appears that Na_2OsO_4 is a metal-stoichiometric Ca_2IrO_4-type compound never been synthesized to date. Na_2OsO_4 has the octahedral environment of $Os^{6+}O_6$ so that the electronic configuration is $5d^2$, suggesting the magnetic $S=1$ ground state. However, magnetization, electrical resistivity, and specific heat measurements indicated that the non-magnetic $S=0$ state is much likely for Na_2OsO_4 than the $S=1$ state. Band structure calculations and the structure analysis found that the disagreement is probably due to the statically uniaxial compression of the OsO_6 octahedra, resulting in splitting of the t_{2g} band.

1. Introduction

The prototype compound Ca_2IrO_4 was described to have "an exceptionally aesthetic crystal structure" in a review article by Müller-Buschbaum in 2003 [1]. This is probably because of the highly artistic projection of the infinite chains comprising IrO_6 octahedra connected by sharing those edges [2–6]. The chains are well separated from each other in a hexagonal symmetry. In our opinion, Ca_2IrO_4 exactly deserves the words.

As suggested by Müller-Buschbaum, fairly few analogue oxides of Ca_2IrO_4 were thus far synthesized, such as $(Ln,Na)_2IrO_4$ (Ln=Gd, Y, Tb, Ho, Dy, Er) [7], $Ba_3Ti_3O_6(BO_3)_2$ [8], $K_3Nb_3O_6(BO_3)_2$ [9], $(Sr,A)_6Bi_3O_{12}$ (A=K, Na) [10], and $K_3Ta_3B_2O_{12}$ [11]. To the best of our knowledge, only the prototype Ca_2IrO_4 crystallizes in the structure without having additional elements such as above. However, Ca_2IrO_4 apparently accommodates a substantial amount of Ca vacancies and the comparable compound $Ca_5Ir_3O_{12}$ seems to be studied instead [2–4]. In turn, the aesthetic structure view is valid only for an ideal compound Ca_2IrO_4, which has never been synthesized to date.

As mentioned, the ideal structure is highly anisotropic, therefore a remarkable quasi-one dimensional magnetism can be expected if it is magnetically active. Besides, unusually anisotropic electrical conductivity can also be expected if it is electrically active. Because both are significant subjects in condensed matter science, we have been searching for additional Ca_2IrO_4-type compounds which are active magnetically or electrically.

Recently, in a course of our studies of the Na–Os–O system [12,13], we apparently synthesized a new Ca_2IrO_4-type compound Na_2OsO_4 under a high-pressure condition. Careful analysis of the structure and the composition revealed that metal-vacancies are quite little. No additional elements were used to synthesize the compound. Na_2OsO_4 thus can be considered as a metal-stoichiometric Ca_2IrO_4-type compound never been synthesized to date. The crystal has the octahedral environment of $Os^{6+}O_6$ so that the electronic configuration is $5d^2$, suggesting the magnetic $S=1$ ground state. In this paper, we report the crystal growth, the crystal

* Corresponding author at: Superconducting Materials Center, National Institute for Materials Science, 1-1 Namiki, Tsukuba, 305-0044 Ibaraki, Japan. Fax: +81 29 860 4674.
E-mail address: yamaura.kazunari@nims.go.jp (K. Yamaura).
[1] Current address: Environmental Molecular Sciences Laboratory, Pacific Northwest National Laboratory, 902 Battelle Boulevard, Richland, WA 99352, USA.

0022-4596/$ - see front matter © 2009 Elsevier Inc. All rights reserved.
doi:10.1016/j.jssc.2009.12.007

structure, and the magnetic and electrical properties of the newly synthesized compound.

2. Experimental

Polycrystalline Na_2OsO_4 was synthesized by means of solid-state reaction under high-pressure. Powders of Na_2O_2 (97%, Sigma-Aldrich) and OsO_2 (Os−84.0%, Alfa Aesar, lot. 039497) were carefully mixed at 15 mol% Na-rich stoichiometry in an Ar-filled dry box, followed by placing into an Au capsule. The capsule was heated at 900 °C for 2.5 h in a high-pressure apparatus, which is capable of maintaining 6 GPa during heating. The capsule was then quenched in the press to ambient temperature before releasing the pressure. The sample was rinsed in water using a sonic bath for few minutes to remove residual ingredients, followed by repeating the rinse. The rinsed powders were dried in air at 140 °C for 10 min. The final products were qualitatively analyzed by a powder X-ray diffraction (XRD) method using Cu$K\alpha$ radiation in a commercial apparatus (RINT 2200 V, RIGAKU), confirming absence of impurities in the sample. The powder was compressed at 6 GPa without heating to form a dense pellet for specific heat (C_p) measurements. It should be noted that preliminary samples heated at much higher temperature comprised mainly the perovskite phase $NaOsO_3$ [12], and other preliminary samples prepared without excess Na_2O_2 contained non-trivial amount of OsO_2.

Single-crystals of Na_2OsO_4 were grown by a NaCl flux method using the polycrystalline sample in the high-pressure apparatus. The polycrystalline Na_2OsO_4 was placed in a Pt capsule with 0.1 mol% of NaCl (99.99%, Rare metallic Co.). The Pt capsule was then heated at 1600 °C for 2.5 h at 6 GPa. The capsule was quenched to ambient temperature before releasing the pressure. The crystals grew as shiny hexagonal rods as shown in Fig. 1a. Perhaps, a small degree of temperature gradient in the Pt capsule played an essential role in growth of the crystal, as was for $NaOsO_3$ [12] and NaV_2O_4 [14].

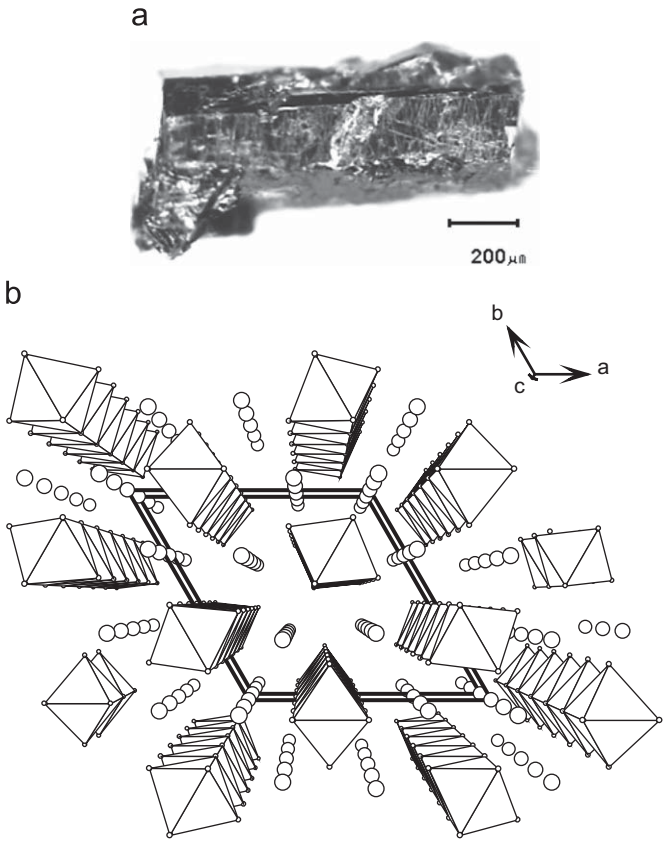

Fig. 1. (a) Photograph of a crystal of Na_2OsO_4 and (b) a structure view. Fat solid lines indicate the hexagonal unit cell.

Table 1
Crystallographic data and structure refinement for Na_2OsO_4.

Empirical formula	Na_2OsO_4
Formula weight	300.18 g/mol
Temperature	290 K
Wavelength	Mo$K\alpha$ (0.71073 Å)
Crystal system	Hexagonal
Space group	$P-62$ m (no. 189)
Unit cell dimensions	a=9.6133(3) Å
	c=3.1567(3) Å
Cell volume	252.64(3) Å^3
Z	3
Density, calculated	5.919 g/cm^3
Crystal size (mm)	0.12 × 0.08 × 0.08
$h\,k\,l$ range	$-16 \le h \le 17,\ -16 \le k \le 17,\ -5 \le l \le 5$
$2\theta_{max}$	80.32
Linear absorption coeff.	37.95 mm^{-1}
Absorption correction	Multi-scan (SADABS; Bruker, 1999)
T_{min}/T_{max}	0.1656/0.3695
No. of reflections	5528
R_{int}	0.0287
No. independent reflections	628
No. observed reflections	560[$F_o > 4\sigma(F_o)$]
F (000)	390
R factors	3.00% (R_1) 6.81% (wR_2)
Weighting scheme	$w=1/[\sigma^2(F_0^2)+(0.0363P)^2+0.16P]$,
	$P=(\mathrm{Max}(F_0^2)+2F_c^2)/3$
Diff. Fourier residues	[−0.90, 5.43] e/Å^3
Refinement software	SHELXL-97

The crystal structure of Na_2OsO_4 was determined by a single-crystal XRD method at ambient temperature and pressure. A crystal of Na_2OsO_4 was mounted on the end of a fine glass fiber on a diffractometer equipped with an area-detector (SMART APEX, Bruker). Monochromatic Mo$K\alpha$ (λ=0.71073 Å) radiation was used. Conditions of the analysis are presented in Table 1. The software packages SMART and SAINT+ were used for the data acquisition and the data extraction/reduction, respectively [15]. An empirical absorption correction was made by the software SADABS [15]. Structure parameters refinement was conducted on the F^2 data by a full-matrix least-squares method using SHELXL-97 [16].

Another crystal was studied by an electron probe micro-analysis (EPMA) (JXA-8500F, JEOL) at the acceleration voltage of 15 kV. Contaminations such as Au/Pt were confirmed below the EPMA background level. The mean metal ratio at 5 points in the sole crystal was Na/Os=2.05(6), suggesting a stoichiometric metal composition. The oxygen content of the crystal was not measured by a chemical method to avoid possible production of the highly toxic OsO_4. Throughout the present study, we assume that the oxygen component is stoichiometric.

Electrical resistivity (ρ) of a selected single-crystal was measured by a four-point method with a dc gauge current of 0.01 mA in a commercial apparatus (Physical Properties Measurement System, Quantum Design) between 2 and 300 K. Electrical contacts on the four locations were prepared by gold wires and silver paste. C_p was measured by a time-relaxation method using the polycrystalline pellet in the apparatus between 2 and 300 K. Magnetic properties were studied in a commercial magnetometer (Magnetic Properties Measurement System, Quantum Design)

using multiple single crystals randomly oriented in a sample holder between 2 and 350 K. Sample holder contribution was carefully subtracted. Applied magnetic field was ± 50 kOe or weaker.

3. Results and discussion

Structural refinements were conducted using the XRD data. We employed the structural model proposed for Ca_2IrO_4 [6] as an initial model, and apparently we succeeded in obtaining a reasonable solution with R factors lower than 7%. The final solutions are summarized in Tables 2 and 3, and calculated bond lengths and bond valence sums are in Table 4. It should be noted that a relatively large Fourier residue found in the analysis ($+5.43\,e/Å^3$) is due to nature of the heavy metal (Os, atomic number: 76). Usually, the value is often smaller than approximately [atomic number]/10 $e/Å^3$ at a 0.6–1.2 Å distance if the structure model is reasonable, hence the present value at 0.6 Å seems to be in a normal range for Os ($< \sim 7.6\,e/Å^3$).

On the way to reach the final solution, we paid large attention on the Na occupancy factor because Ca vacancies at the same crystallographic site (1a site in Wyckoff position) were found to be substantial in the prototype compound Ca_2IrO_4 [2–4]. First, we fixed the 1a occupancy factor at zero, resulted in only unsatisfactory solutions. We then investigated a difference Fourier map and found that an atom is obviously at the 1a site. Afterwards, we unfixed the occupancy factor of the 1a site, leading a remarkable improvement of the refinement quality. The occupancy factor was 0.99(2), indicating that the 1a site is fully occupied by Na. Thus, we fixed the occupancy factor of Na1 (1a site) fully occupied in the last refinement. Because no unusual thermal parameters were detected (Table 3), the EPMA result is consistent with the stoichiometric Na concentration, and the bond valance sums (Table 4) are consistent with the expectation, we believe that the crystal of Na_2OsO_4 is highly stoichiometric in metals, unlike what was found for Ca_2IrO_4.

Fig. 1b shows a projection of the crystal structure along the chain direction. The chain comprising OsO_6 octahedra runs along the c-axis by sharing those edges. The chains are well-separated from each other by Na atoms (the inter-chain Os–Os distance is 5.58 Å, being 1.77 times longer than the intra-chain Os–Os distance). The local chain structure is depicted in Fig. 2a. We found the octahedral OsO_6 distorts uniaxially in a notable way: the shortest and longest Os–O bonds are 16% different in distance (see Fig. 2b), being remarkable than 3.2% for $Ca_{2-x}IrO_4$ [3]. Because of the large magnitude of the axial compression, we expected that the degeneracy of the $5d_{xy}$ and $5d_{yz}$ ($5d_{zx}$) orbital is broken, as sketched out in Fig. 2c. The axial compression along z direction (defined parallel to the Os–O3 bond) should render the

Table 2
Structure parameters of Na_2OsO_4.

Site	Wyckoff position	x	y	z	U_{eq}
Os	3f	0.32963(2)	0	0	0.0129(1)
Na1	1a	0	0	0	0.020(1)
Na2	2d	1/3	2/3	0.5	0.025(1)
Na3	3g	0.6943(4)	0	0.5	0.020(1)
O1	3g	0.1935(5)	0	0.5	0.018(1)
O2	3g	0.4580(5)	0	0.5	0.017(1)
O3	6j	0.4308(5)	0.2127(4)	0	0.031(1)

Table 3
Anisotropic displacement parameters (Å^2) of Na_2OsO_4.

Atom	U_{11}	U_{22}	U_{33}	U_{12}
Os	0.01341(10)	0.01360(12)	0.01176(12)	0.00680(6)
Na1	0.0215(16)	0.0215(16)	0.017(3)	0.0107(8)
Na2	0.0265(17)	0.0265(17)	0.023(3)	0.0133(8)
Na3	0.0205(10)	0.0229(19)	0.018(2)	0.0115(10)
O1	0.0151(15)	0.020(3)	0.022(4)	0.0099(13)
O2	0.0164(15)	0.026(3)	0.014(3)	0.0129(13)
O3	0.049(3)	0.0147(14)	0.0131(19)	0.004(2)

$U_{13}=U_{23}=0$ for all the atoms.

Table 4
Bond lengths, l (Å), and bond valence sums, BVS [17],[a] in Na_2OsO_4.

Bonds	l and BVS	Bonds	l and BVS
Os–O3 ($\times 2$)	1.772(3)	Na2–O3 ($\times 6$)	2.519(4)
Os–O2 ($\times 2$)	2.004(3)	Na2–O2 ($\times 3$)	2.8043(8)
Os–O1 ($\times 2$)	2.050(3)	BVS(Na2)	1.06
BVS(Os)	6.07	Na3–O2	2.271(7)
Na1–O1 ($\times 6$)	2.440(4)	Na3–O3 ($\times 4$)	2.411(4)
BVS(Na1)	1.06	Na3–O1 ($\times 2$)	2.575(3)
		BVS(Na3)	1.29

[a] $BVS=\Sigma v_i$, $v_i=\exp[(R_0-l_i)/B]$, $B=0.37$, $R_0(Na^+)=1.80$, and $R_0(Os^{6+})=1.925$. The $R_0(Os^{6+})$ was estimated by a linear extrapolation from the experimental values of $R_0(Os^{4+})$ and $R_0(Os^{5+})$ [18].

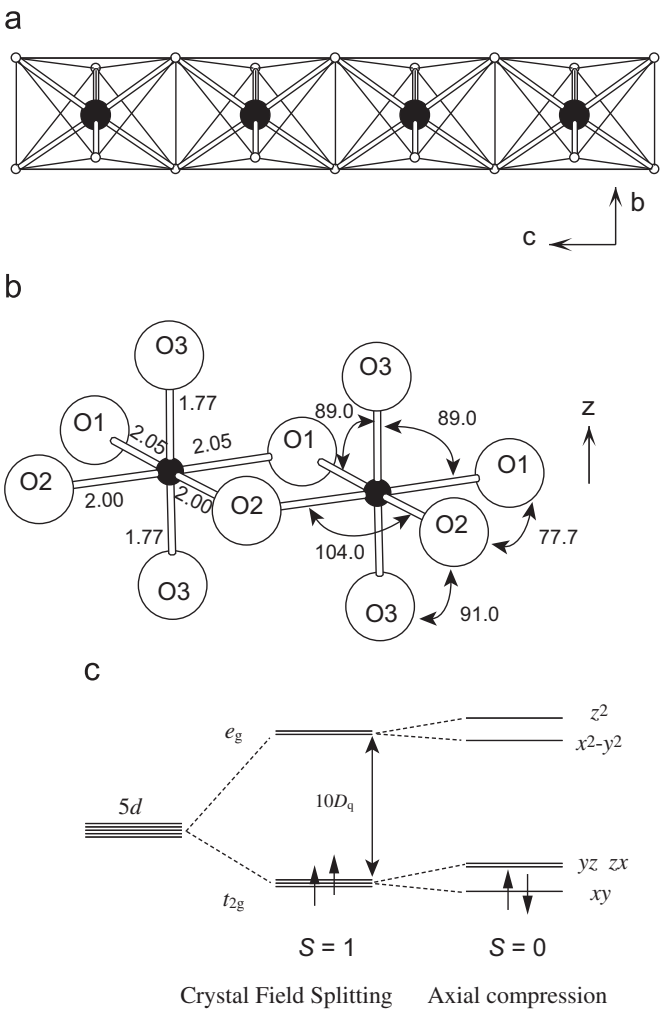

Fig. 2. (a) Local structure of the chain and (b) the OsO_6 octahedra. Numbers are bond distances in Å and bond angles in degrees. (c) 5d bands scheme expected for Na_2OsO_4.

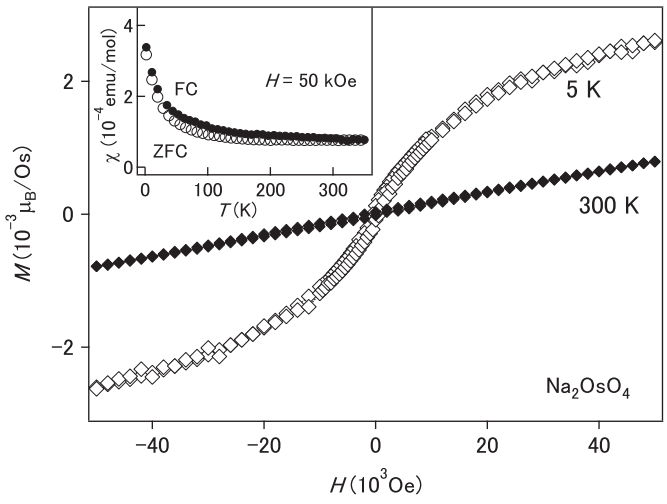

Fig. 3. Magnetic field dependence of the magnetization and (inset) temperature dependence of the magnetic susceptibility of Na_2OsO_4.

$5d_{xy}$ level lower in energy than the $5d_{yz}$ and $5d_{zx}$ levels. Thus, it is reasonable to expect that the magnetic ground state is $S=0$ ($5d^2_{xy}5d^0_{yz}5d^0_{zx}$) rather than $S=1$ ($5d^1_{xy}5d^1_{yz}5d^0_{zx}$ or $5d^1_{xy}5d^0_{yz}5d^1_{zx}$).

Temperature dependence of the magnetic susceptibility (χ) is shown in the inset to Fig. 3. The sample consisted of randomly oriented crystals measured. It is obvious that χ is nearly temperature-independent with a small magnitude of $\sim 1\times10^{-4}$ emu/mol, suggesting a spin moment is almost absent. This well accords with the non-magnetic model ($S=0$). The broad and small upturn in low temperature was observed in additions to the weak separation between the ZFC and FC curves. This is possibly due to a surface matter, where axial compression may be relaxed and spins emerge restrictively. Otherwise, undetected magnetic impurities such as $NaOsO_3$ [12] or Na_3OsO_5 [19] may be locally formed and account for the temperature dependence.

Although the 5 K magnetization curve shows a positive curvature (Fig. 3), it likely reflects the impurities contribution because it is fairly small ($<\sim 3\times10^{-3}\,\mu_B$/Os). Alternatively, it is possible that a transition from the $S=0$ state to the $S=1$ state is gradually induced in the applied magnetic field, accounting for the positive curvature. Further high-magnetic field studies can correctly estimate the possible magnetic activation. The observed properties are rather consistent with the non-magnetic picture ($S=0$) than the magnetic picture ($S=1$).

Fig. 4 shows ρ of the Na_2OsO_4 crystal measured along the chain (c-axis). As the crystal is a hexagonal rod, the chain runs along the longitudinal direction as found for $Ca_{2-x}IrO_4$ [2]. Over the studied range between 2 and 300 K, ρ continuously increases as T decreases as expected for a semiconducting feature, while ρ at room temperature is relatively low ($\sim$4.5 Ω cm). To further analyze the temperature dependence, the data are plotted in the variable range hopping (VRH) form. The VRH plot appears to be almost linear, suggesting that the VRH conduction is dominant in the charge transport of Na_2OsO_4.

Fig. 5 shows temperature and magnetic field dependence of C_p of Na_2OsO_4. We analyzed the low-temperature C_p by applying the approximated Debye model $C(T)/T=\beta T^2+\gamma$, where β is a coefficient and γ is the electronic-specific-heat coefficient. The analysis is expected to be valid in the low temperature range $T<<T_D$ (the Debye temperature). The C_p/T vs. T^2 plot below 4.5 K indeed appear to be linear as expected (see inset to Fig. 5), hence we fit to the part, yielding β of $3.50(8)\times10^{-4}$ J mol^{-1} K^{-4} and γ of 2.1(1) mJ mol^{-1} K^{-2}. We obtained T_D of 339(2) K from the β. C_p in a magnetic field of 70 kOe was analyzed as well, yielding β of

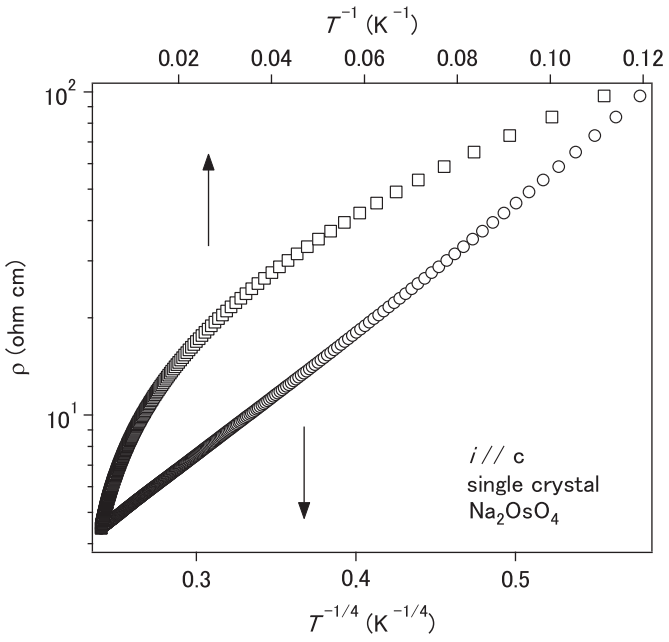

Fig. 4. Temperature dependence of the electrical resistivity of Na_2OsO_4 along the chain direction, plotted in ρ vs. T^{-1}(top axis) and ρ vs. $T^{-1/4}$ (bottom axis).

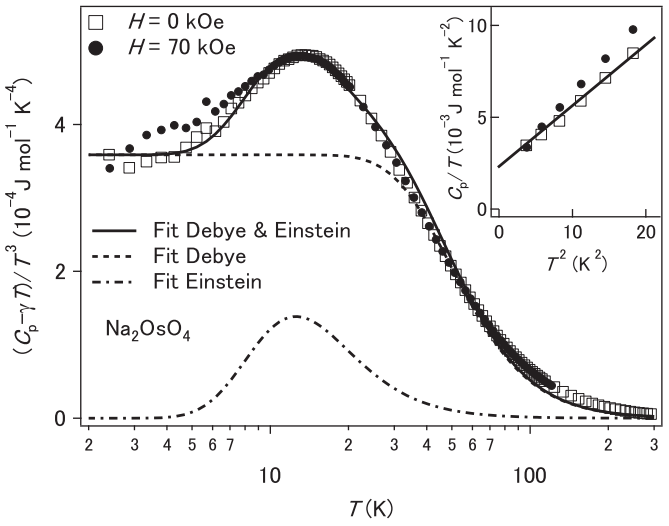

Fig. 5. Lattice specific heat of Na_2OsO_4. Line and curves indicate fits to the 0 kOe data.

$4.38(8)\times10^{-4}$ J mol^{-1} K^{-4} [T_D of 314(2) K] and γ of 1.9(1) mJ mol^{-1} K^{-2}, indicating that the magnetic field dependence of the thermo-dynamical parameters is insignificant. This well accords with the non-magnetic picture.

Subsequently, the entire part of the C_p ($<$300 K) was quantitatively analyzed by using a linear combination of the Debye model, the Einstein model, and the electronic specific heat, as it successfully fit to C_p of the osmium oxides, including KOs_2O_6 and $RbOs_2O_6$ [20]. The data are plotted in the lattice specific heat $(C_p-\gamma T)/T^3$ vs. T in Fig. 5. The analytical formula was

$$C(T)=n_D\times 9N_Ak_B\left(\frac{T}{T_D}\right)^3\int_0^{T_D/T}\frac{x^4e^x}{(e^x-1)^2}dx+n_E \times 3N_Ak_B\left(\frac{T_E}{T}\right)^2\frac{e^{T_E/T}}{(e^{T_E/T}-1)^2}+\gamma T,$$

where N_A is Avogadro's constant, k_B is Boltzmann's constant, and T_E is the Einstein temperature. The scale factors n_D and n_E correspond to the number of vibrating modes per the formula unit in the Debye and the Einstein models, respectively. Fit to the data yielded T_D of 244(2) K, T_E of 61.9(8) K, n_D of 2.66(7), and n_E of 0.062(3). The Einstein contribution appears as a broad peak in the lattice plot. The non-trivial Einstein term suggests that anharmonic lattice dynamics somewhat exist in Na_2OsO_4. To further investigate the lattice specific heat, C_p was measured in the magnetic field of 70 kOe as well. The fits to the data yielded T_D of 236(3) K, T_E of 59(1) K, n_D of 2.56(8), and n_E of 0.045(3), indicating little change. The insignificant magnetic field dependence of C_p is in a good accordance with the non-magnetic picture. Additional studies are needed to identify the origin of the possible anharmonic dynamics in Na_2OsO_4.

We studied the electronic structure of Na_2OsO_4 using the local density approximation (LDA) [21] of density functional theory [22]. We used WIEN2k package [23], which is based on a full-potential augmented-plane-wave method. Experimental lattice parameters and atomic coordinates were used with the atomic radii of 2.0, 1.8, and 1.7 a.u. for Na, Os, and O, respectively. The cut-off wave-number K for wave functions in interstitial region was set to $RK=7$, where R is the smallest atomic sphere radius. The integration over Brillouin zone was performed by a tetrahedron method with 144 k-points in the irreducible Brillouin zone.

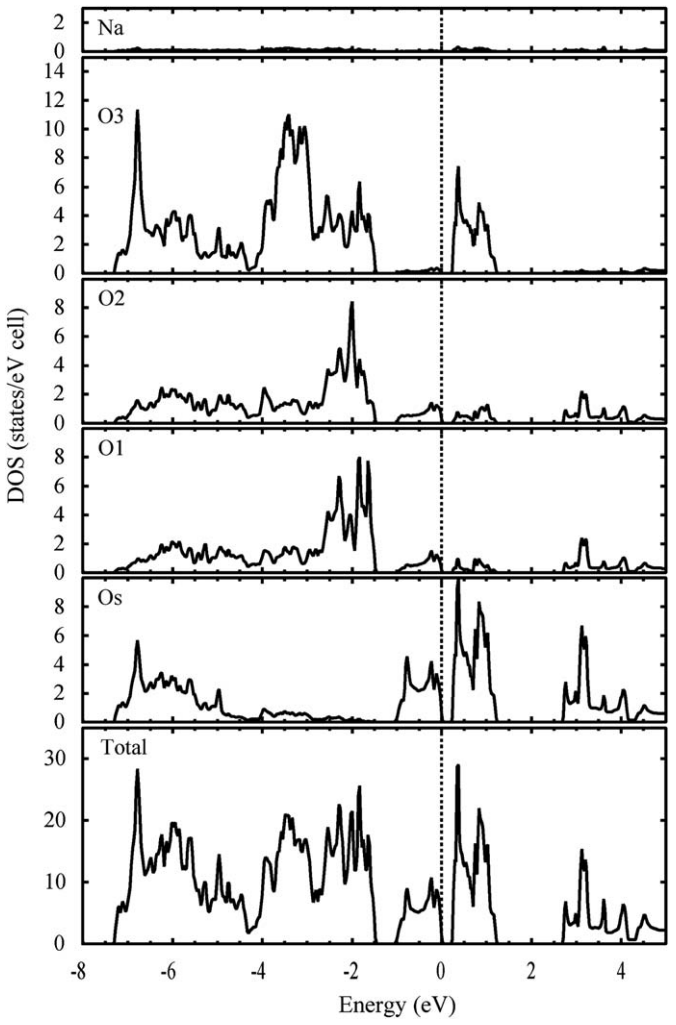

Fig. 6. Non-magnetic DOS of Na_2OsO_4 with SO couplings. Dotted line indicates the valence band top.

We calculated density of state (DOS) with spin–orbit (SO) couplings because they possibly affect qualitatively and quantitatively the electronic structure, as extensively discussed for the 5*d* oxide Sr_2IrO_4 [24]. As a result, we did not see any remarkable differences in the solutions with and without the SO couplings unlike what was found for Sr_2IrO_4. The DOS shown in Fig. 6 was calculated with the SO couplings. We found the Os t_{2g}-bands distribute between -1.0 and 1.2 eV, and it is notable that a gap opens at the top of the valence band in the t_{2g} structure. The gap was found without considering any spin arrangements, indicating that the crystal is semiconducting or insulating in nature. Thus, the static structure origin, i.e. axial compression of the OsO_6 octahedra (see Figs. 2a–c), is most likely responsible for the gap opening. Because of the gapped electronic structure, the nominal configuration of Os^{6+} with $5d^2$ is reasonably expected to form a paired electrons in the 5*d xy* orbital (see Fig. 2c), resulting in the non-magnetic ground state of $S=0$.

4. Conclusions

The first principles calculation suggested the non-magnetic ground state ($S=0$) for the $5d^2$ oxide Na_2OsO_4 rather than the magnetic state ($S=1$), and it is indeed consistent with the observed properties. The structure analysis and the first principles study suggested that the uniaxial compression of the OsO_6 octahedra is essential to establish the non-magnetic state. Unlike what was observed for such as d^4(high-spin), d^7, and d^9 oxides, Jahn-Teller effect alone unlikely accounts for the local distortion [25]. Since we have quite few 5*d* oxides to display such the dramatically uniaxial compression effect in magnetism, Na_2OsO_4 thus provides valuable opportunities to advance further understanding of nature of the 5*d* oxides.

Although a band-gap at the valence band top was found in the t_{2g} DOS structure, small γ ($\sim 2\,mJ\,mol^{-1}\,K^{-2}$) was actually detected at the lowest temperature limit, indicating small DOS remains. The observed VRH conduction is probably related to the residual DOS, in which charge carriers are largely scattered by disorder. The small disagreement between the observed and the calculated DOS at the valence band top is an issue left for future study. It would also be interesting to investigate the crystal under physical or chemical pressures because those may change the degree of the uniaxial compression, resulting in appearance of the magnetic $S=1$ state. Because magnetism of the well-separated chains in the hexagonal arrangement is of great interest, further studies toward activating the magnetism state are in progress.

Acknowledgments

We thank K. Kosuda for the EPMA. This research was supported in part by the WPI Initiative on Materials Nanoarchitectonics from MEXT, Japan, and the Grants-in-Aid for Scientific Research (20360012) from JSPS. Work at Argonne National Laboratory supported under Contract no. DE-AC02-06CH11357 by UChicago Argonne, LLC, Operator of Argonne National Laboratory, a US Department of Energy Office of Science Laboratory.

References

[1] H.K. Müller-Buschbaum, J. Alloys Comp. 349 (2003) 49.
[2] G. Cao, V. Durairaj, S. Chikara, S. Parkin, P. Schlottmann, Phys. Rev. B 75 (2007) 134402.
[3] M. Wakeshima, N. Taira, Y. Hinatsu, Y. Ishii, Solid State Commun. 125 (2003) 311.

[4] F.J.J. Dijksma, J.F. Vente, E. Frikkee, D.J.W. Ijdo, Mater. Res. Bull. 28 (1993) 1145.
[5] R.F. Sarkozy, C.W. Moeller, B.L.J. Chamberland, Solid State Chem. 9 (1974) 242.
[6] V.D. Babel, W. Rüdorff, R.Z. Tschöpp, Anorg. Allg. Chem. 347 (1966) 282.
[7] S.J. Mugavero III, M.D. Smith, H.-C. zur Loye, Solid State Sci. 9 (2007) 555.
[8] H.-S. Park, A. Bakhtiiarov, W. Zhang, I. Vargas-Baca, J. Barbier, J. Solid State Chem. 177 (2004) 159.
[9] P. Becker, L. Bohaty, J. Schneider, Kristallografiya 42 (1997) 250.
[10] J.S. Pshirkov, S.M. Kazakov, A.M. Abakumov, S.N. Putilin, E.V. Antipov, C. Bougerol-Chaillout, O.I. Lebedev, G.J. van Tendeloo, Solid State Chem. 152 (2000) 492.
[11] S.C. Abrahams, L.E. Zyontz, J.L. Bernstein, J.P. Remeika, A.S.J. Cooper, Chem. Phys. 75 (1981) 5456.
[12] Y.G. Shi, Y.F. Guo, S. Yu, M. Arai, A.A. Belik, A. Sato, K. Yamaura, E. Takayama-Muromachi, H.F. Tian, H.X. Yang, J.Q. Li, T. Varga, J.F. Mitchell, S. Okamoto, Phys. Rev. B 80 (2009) 161104(R).
[13] Y.G. Shi, A.A. Belik, M. Tachibana, M. Tanaka, Y. Katsuya, K. Kobayashi, K. Yamaura, E.J. Takayama-Muromachi, Solid State Chem. 182 (2009) 881–887.
[14] K. Yamaura, M. Arai, A. Sato, A.B. Karki, D.P. Young, R. Movshovich, S. Okamoto, D. Mandrus, E. Takayama-Muromachi, Phys. Rev. Lett. 99 (2007) 196601;
K. Yamaura, M. Arai, A. Sato, A.B. Karki, D.P. Young, R. Movshovich, S. Okamoto, D. Mandrus, E. Takayama-Muromachi, Phys. Rev. Lett. 101 (2008) 129901.
[15] SMART, SAINT+, and SADABS packages, Bruker Analytical X-ray Systems Inc., Madison, WI, 2002.
[16] G.M. Sheldrick, SHELXL97 Program for the Solution and Refinement of Crystal Structures, University of Göttingen, Germany, 1997.
[17] I.D. Brown, Acta Crystallogr. B 33 (1977) 1305.
[18] J. Yamaura, S. Yonezawa, Y. Muraoka, Z.J. Hiroi, Solid State Chem. 179 (2006) 336.
[19] K.M. Mogare, W. Klein, H. Schilder, H. Lueken, M.Z. Jansen, Anorg. Allg. Chem. 632 (2006) 2389.
[20] M. Bruhwiler, S.M. Kazakov, N.D. Zhigadlo, J. Karpinski, B. Batlogg, Phys. Rev. B 70 (2004) 020503R.
[21] J.P. Perdew, Y. Wang, Phys. Rev. B 45 (1992) 13244.
[22] P. Hohenberg, W. Kohn, Phys. Rev. 136 (1964) B864.
[23] P. Blaha, K. Schwarz, G.K.H. Madsen, D. Kvasnicka, J. Luitz, WIEN2k, An Augmented Plane Wave+Local Orbitals Program for Calculating Crystal Properties, Karlheinz Schwarz, Technische Universitat Wien, Austria, 2001.
[24] B.J. Kim, H. Jin, S.J. Moon, J.-Y. Kim, B.-G. Park, C.S. Leem, J. Yu, T.W. Noh, C. Kim, S.-J. Oh, J.-H. Park, V. Durairaj, G. Cao, E. Rotenberg, Phys. Rev. Lett. 101 (2008) 076402.
[25] R. Janes, E.A. Moore, Metal–ligand bonding, Royal Society of Chemistry, Great Britain, Open University, 2004.